# Hot corrosion of $Gd_2Zr_2O_7$, $Gd_2Zr_2O_7$/YbSZ, YSZ + $Gd_2Zr_2O_7$/YbSZ, and YSZ thermal barrier coatings exposed to $Na_2SO_4$ + $V_2O_5$

Mohadese Tabeshfar [a,b], Mehdi Salehi [a], Ghasem Dini [c], Paul Inge Dahl [d], Mari-Ann Einarsrud [b], Kjell Wiik [b,*]

[a] *Department of Materials Engineering, Isfahan University of Technology, Isfahan 84156-83111, Iran*
[b] *Department of Materials Science and Engineering, NTNU Norwegian University of Science and Technology, 7491 Trondheim, Norway*
[c] *Department of Nanotechnology, Faculty of Chemistry, University of Isfahan, Isfahan 81746-73441, Iran*
[d] *Department of Sustainable Energy Technology, SINTEF Industry, 7031 Trondheim, Norway*

## ARTICLE INFO

## ABSTRACT

$Gd_2Zr_2O_7$ ceramic is considered as a potential candidate for thermal barrier coatings. Here we present hot corrosion behavior of single layer $Gd_2Zr_2O_7$ (GZO), $Gd_2Zr_2O_7$ + 50 wt% YbSZ (GZO/YbSZ), YSZ and double-layer YSZ/$Gd_2Zr_2O_7$ + 50 wt% YbSZ (YSZ + GZO/YbSZ) coatings prepared by air plasma spraying on Inconel 625 substrates. Prior to hot corrosion the fracture toughness of the coatings was assessed by Vickers indentation showing a variation between 0.6 and 2.3 $MPa \cdot m^{1/2}$ where the GZO/YbSZ coating exhibited the highest fracture toughness. The hot corrosion test was conducted by exposing the coatings to an equimolar mixture of $Na_2SO_4$ and $V_2O_5$ at 750 °C. After the hot corrosion test, the type of phases, chemical composition, microstructure and crack formation were investigated. Formation of $GdVO_4$ and $YVO_4$ was observed as the corrosion products in the GZO containing coatings and the YSZ coating, respectively. All coatings showed the formation of monoclinic zirconia after the corrosion test. The $Gd_2Zr_2O_7$ + 50 wt% YbSZ (GZO/YbSZ) coating showed the best hot corrosion resistance due to reduced reactivity and enhanced fracture toughness and represents a new composition with properties promising for TBC applications.

## 1. Introduction

Air plasma sprayed thermal barrier coatings (TBCs) are used as thermal insulation multilayer systems to protect hot section parts of gas turbine engines [1,2]. A typical TBC system includes three layers: 1) a metallic bondcoat as an oxidation/corrosion-resistant layer, 2) a thermally grown oxide (TGO) layer formed as an oxidation product between the topcoat and the bondcoat mainly consisting of alpha-alumina ($\alpha$-$Al_2O_3$) and small amounts of other oxides and 3) a ceramic topcoat as a thermal insulation layer [3,4]. TBCs have been widely used in gas turbine engine components such as turbine vanes and blades to protect them from harsh environment, improving thermal insulation at high temperatures and increasing the operating temperature and efficiency [5,6]. The most commonly used ceramic topcoat material is 7–8 wt% yttria-stabilized zirconia (YSZ). Despite notable thermomechanical properties, the application of YSZ is limited to temperatures <1200 °C due to enhanced sintering, CMAS (calcium-magnesium- aluminosilicate) infiltration and a 3–5 vol% expansion during the phase transformation from tetragonal (t′) to monoclinic zirconia upon cooling [7–9]. Therefore, rare earth zirconates (e.g. $Gd_2Zr_2O_7$) with lower thermal

conductivity, higher melting point, higher chemical stability and better ability to accommodate defects than YSZ have received increasing attention as new materials for thermal barrier coatings [6,10]. In particular, $Gd_2Zr_2O_7$ (GZO) does not have any destructive phase transformations at higher temperatures as opposed to YSZ and the order-disorder phase transformation has no significant influence on the integrity of the coating [11]. However, GZO reacts with the TGO layer at high temperatures forming an undesirable porous $GdAlO_3$ perovskite structured phase that compromises the integrity of the TBC [11–13].

TBCs are normally applied by using air plasma spraying (APS), vacuum plasma spraying, high-velocity oxygen fuel (HVOF) thermal spraying, and electron beam physical vapor deposition (EB-PVD) techniques [12,13]. Even though EB-PVD gives coatings with higher strain tolerance and thermal cyclic oxidation life, APS is a more cost-effective and fast deposition method with higher deposition efficiency and thermal insulation properties compared to the other methods [5,13,14]. Therefore, the APS method was selected for applying the coatings in this study.

TBCs are prone to different failure mechanisms, such as erosion, thermal shock, oxidation, and hot corrosion. Harsh operating conditions can affect the performance of the thermal barrier coating, espe-

* Corresponding author.
   *E-mail address:* kjell.wiik@ntnu.no (K. Wiik).

cially hot corrosion. Impurities like vanadium and sulphur contaminants from low-quality fuels combine to form molten sulfate-vanadate deposits that are extremely corrosive [5,15,16]. The main reason for the failure of the YSZ topcoat is the reaction of the molten or semi-molten salts with yttria in YSZ, leaching yttria from the zirconia. Hence, phase transformation of tetragonal prime to monoclinic zirconia occurs during cooling followed by cracking and spallation of the different layers of the TBC [12,17]. Efforts to improve the phase stability and hot corrosion resistance of YSZ ceramics include doping YSZ with more acidic stabilizer oxides such as $In_2O_3$, $Sc_2O_3$ and $CeO_2$ [3,18]. Further, thermophysical properties of $RE_2O_3$ (RE = Dy, Y, Er, Yb) stabilized zirconia have been investigated [21–22] showing that YbSZ (3.5–5 mol% $Yb_2O_3$) has the best phase stability and fracture toughness among them [19,20]. YbSZ (3.5 mol% $Yb_2O_3$ in $ZrO_2$) is known for its high fracture toughness reaching 5.17 MPa·m$^{1/2}$ [19], a lower sintering rate and a higher thermal expansion coefficient ($11.25 \cdot 10^{-6}$ K$^{-1}$ at 1200 °C) compared to YSZ (between ~10 and 11 × 10$^{-6}$ K$^{-1}$) [21,22]. However, the hot corrosion resistance behavior of YbSZ has not been reported. In addition, the new alternative topcoat materials such as rare earth zirconates are expected to have improved performance (longer life) at hot corrosion conditions compared to stabilized zirconia, due to higher stability and less reactivity with corrosive components. Hence, the application of rare earth zirconates is a promising approach to enhance the hot corrosion resistance of TBCs [17,23].

There are a few reports on the hot corrosion behavior of air plasma sprayed Gadolinium zirconate (GZO) + rare earth stabilized zirconia (RESZ) coatings against different corrosive environments at different temperatures. Marple et al. [24] and Yugeswaran et al. [15] indicated that APS applied $La_2Zr_2O_7$ coatings exposed to $V_2O_5$ were resistant to hot corrosion at 1000 and 1075 °C, respectively [24]. Also, the hot corrosion resistance of GZO was investigated at temperatures between 650 and 1050 °C [6,9], and showed an enhanced corrosion resistance to $Na_2SO_4$ + $V_2O_5$ compared with YSZ [11]. Habibi et al. [6] investigated the hot corrosion behavior of GZO, YSZ and GZO + YSZ composite coatings in the presence of a molten mixture of $Na_2SO_4$ + $V_2O_5$ at 1050 °C. They demonstrated that GZO coatings were more thermally and chemically stable and exhibited a better hot corrosion resistance than YSZ coatings. In contrast to Habibi's result, Mahade et al. reported that GZO + YSZ composite coatings showed better hot corrosion resistance compared to pure GZO when exposed to $V_2O_5$ and $Na_2SO_4$ [8].

Jonnalagadda et al. [25] investigated suspension plasma sprayed composite coatings of GZO + YSZ with the intention to improve fracture toughness and hot corrosion resistance. The effect of columnar microstructure and a sealing layer of GZO on the corrosion damage in the presence of a $Na_2SO_4$ + NaCl salt mixture showed that the columnar gaps in the coating served as effective pathways for the molten salt infiltration. The most severe attacks were due to overflow of molten salts to the side surfaces followed by corrosion damage from the edge to the coating center.

In the present investigation we take advantage of the improved stability and hot corrosion resistance of GZO [6,9,10] and add 50 wt% (82 mol%) YbSZ with 5 mol% $Yb_2O_3$ (notation GZO/YbSZ) with the intention to improve both mechanical properties [19,20] and corrosion resistance of the topcoat. To the best of our knowledge this is the first-time GZO with 50 wt% YbSZ has been investigated. The hot corrosion properties were assessed at 750 °C on topcoat layers applied by APS on a nickel-based superalloy (IN-625) using an equimolar mixture of $V_2O_5$ and $Na_2SO_4$. To elucidate the corrosion mechanisms, similar experiments were conducted with three other topcoats, pure GZO, pure YSZ and a combination of YSZ and GZO/YbSZ. The variation in hot corrosion behavior between the different topcoat compositions is discussed and corrosion/failure mechanisms are proposed.

## 2. Material and methods

### 2.1. Synthesis of GZO and GZO/YbSZ

$Yb_2O_3$-stabilized $ZrO_2$ powder (5 mol% $Yb_2O_3$ in $ZrO_2$, notation YbSZ) was prepared by co-precipitation [19]. $Yb_2O_3$ (Wanfeng Adv. Materials Tech. Co., Ganzhou (Jiangxi), China; purity ≥99.998%) and $ZrOCl_2.8H_2O$ (Merck, Darmstadt, Germany; purity ≥99.0%) were selected as starting materials and appropriate amounts were dissolved in hot dilute nitric acid, and deionized water (molality of the solutions corresponded to 0.015 mol/kg and 0.31 mol/kg, respectively). The solutions were mixed together under stirring to obtain a homogeneous solution. The resultant solution was added drop by drop to an excess ammonia solution (pH > 12), and homogeneous gel-like precipitates were obtained. The precipitates were filtered and washed with distilled water and ethanol until the pH value reached 7 [26]. The obtained powder was dried at 110 °C for 18 h and subsequently calcined in air at 800 °C for 5 h.

The $Gd_2Zr_2O_7$ powder (GZO) was fabricated by the solid-state reaction method [30–31]. A mixture of $Gd_2O_3$ (Wanfeng Adv. Materials Tech. Co., Ganzhou (Jiangxi), China; purity ≥99.999%) and $ZrO_2$ (Sigma Aldrich, Taufkirchen, Germany, purity ≥99%, 5 μm) powders with a weight ratio of 1.47 was mechanically milled in a high energy planetary ball mill (Retsch PM100, Haan, Germany) in ethanol using zirconia balls (15 mm diameter) for 24 h. The milled powder was heat treated in air at 1600 °C for 5 h (heating and cooling rates 200 °C/h).

Weight ratio 1:1 of GZO and YbSZ powders (GZO/YbSZ), corresponding to 82 mol% YbSZ, were mixed by ball milling with zirconia balls. The bond coat was a NiCrAlY alloy with agglomerate size between 53 and 105 μm and composition 67 at.% Ni, 10 at.% Cr, 22 at.% Al and 1 at.% Y (PAC 9620 AM, Loveland, OH, USA). Commercial 8 wt% $Y_2O_3$ stabilized $ZrO_2$ (4.5 mol% $Y_2O_3$ in $ZrO_2$) powder with agglomerate size between 15 and 140 μm was provided by PAC 2008P (Loveland, OH, USA) and used for plasma spraying the YSZ topcoat. The GZO powder and GZO/YbSZ powder mixtures were spray dried (4 M8-Trix Formatrix, ProCepT, Zelzate, Belgium) from aqueous slurries containing polyvinyl alcohol (PVA, Merck, Darmstadt, Germany; CAS NO: 9002-89-5) as a binder to increase the strength of the agglomerates. Prior to spray drying the slurries contained typically 30 wt% solid loading, 5 wt% PVA and water. The processing parameters used during the spray drying are given in Table 1. To prevent sedimentation of the powders, the slurries were stirred during the spray drying.

### 2.2. Air plasma spraying (APS)

Nickel-based superalloy (IN-625) specimens as substrate were prepared in a semi-circle shape with diameter and thickness of 16 and 5 mm, respectively. In order to increase the surface roughness and coating adhesion, the substrates were grit blasted by SiC particles (25 μm) and cleaned with ethanol prior to air plasma spraying a ~ 100 μm coating of NiCrAlY. Further, topcoats of the spray dried powders were applied onto the as-sprayed NiCrAlY bond-coat with thickness ~ 200 μm for GZO and YSZ, and ~ 300 μm for GZO/YbSZ. The thickness of each layer of the double layered YSZ + GZO/YbSZ coating was ~200 and ~ 100 μm, respectively. APS of all coatings was

**Table 1**
Processing parameters used during the spray drying.

| Material | Temperature of inlet air (°C) | Nozzle pressure (bar) | Nozzle orifice size (mm) | Feed rate (mL/min) |
|---|---|---|---|---|
| GZO | 170 | 12 | 1.2 | 7.2 |
| GZO/YbSZ | 160 | 10 | 1.2 | 9.0 |

conducted by a company in Iran (Poudrafshan Company, Baharestan Street 46, Dolatabad Industrial Zone, Isfahan, Iran) and the parameters used are given in Table 2.

### 2.3. Hot corrosion test

In order to investigate the hot corrosion behavior of the different coatings, the surface of each topcoat was covered uniformly (~10 mg/cm$^2$) with a homogeneous mixture of 55 wt% $V_2O_5$ (Sigma Aldrich, Taufkirchen, Germany, purity 99.95%) and 45 wt% $Na_2SO_4$ (Merck, Darmstadt, Germany, purity ≥99.0%), corresponding to an equimolar ratio between $V_2O_5$ and $Na_2SO_4$ [27]. The edge of each sample (~3 mm) was uncoated to prevent edge effects [12,13]. The samples were heated in an electric furnace at 750 °C for 3, 6, 12, 18 and 24 h with heating and cooling rates of 200 °C/h. In order to check the reproducibility, two samples of each type of topcoat were corrosion tested and characterized.

### 2.4. Coating characterization

#### 2.4.1. Microscopic analysis

Field emission scanning electron microscope (FESEM/EDS, Zeiss ULTRA 55, Oberkochen, Germany) was used to evaluate the morphology, microstructure, and composition of the surface and cross-section of the samples. The samples were mounted in an epoxy resin and polished to examine the cross-sections. The porosity of the different layers of the coatings was measured by Image J software of the cross-section micrographs.

#### 2.4.2. XRD analysis and Raman spectroscopy

X-ray diffraction (XRD) patterns in the 2θ-range 20–90°, step size of 0.013°, and counting time 57.6 s/step were recorded by a Bruker D8 DaVinci diffractometer with Cu-Kα radiation (Billerica, Massachusetts, USA) to analyze the crystallographic structure and phase distribution at the surface of the coatings before and after the hot corrosion test. Raman spectra were recorded by a confocal Raman spectrometer (Witech, Alpha 300, Ulm, Germany) in a backscattering geometry with a spectral resolution of 1 cm$^{-1}$ over a range from 100 to 3800 cm$^{-1}$ with an excitation wavelength of 532 nm (frequency-doubled Nd-YAG laser operating at 66 mW power). Illumination and detection were performed through a microscope objective at 50× magnification and a numerical aperture of 0.75.

### 2.5. Fracture toughness

Polished cross sections of all coatings were indented with Vickers indentation (Wolpert, Dia tester 2RC-S, Langenfeld, Germany) to calculate the fracture toughness using Eq. (1) [19].

$$K_{IC} = 0.16 \, H_V a^2 c^{-3/2} \tag{1}$$

where $H_v$ is the microhardness, $a$ is the half-length of the indent diagonal (μm), $c$ is the half crack length measured from the middle of the indent to the tip of the crack (μm). A force corresponding to 1 kg was applied for 15 s to develop indentation cracks. Five indents were made for each coating and the average is reported. Diagonal size and crack length of the indent were measured by SEM (Philips, XI30, Eindhoven, The Netherlands).

## 3. Results

### 3.1. Microstructure of the spray dried powders

The spray dried powders have a spherical or semi-spherical morphology and an agglomerate size between 10 and 70 μm (Fig. 1). The powders were subsequently sieved and the fraction > 20 μm was used for plasma spraying.

### 3.2. Characterization of as-sprayed coatings

The XRD pattern of the as-sprayed GZO coating is provided in Fig. 2a and the presence of the low intensity diffraction lines is shown in the enhanced section and indicate the formation of a single pyrochlore phase. The Raman spectrum in Fig. 2b, showing the bands of the pyrochlore phase [28], confirms the presence of a single pyrochlore phase.

The Raman spectrum of the mechanically mixed GZO and YbSZ powders prior to plasma spraying is shown in Fig. 3b (black curve) and the presence of a tetragonal phase (YbSZ) and a pyrochlore phase (GZO) is evident. The XRD pattern of the as plasma sprayed GZO/YbSZ is given in Fig. 3a and shows the presence of a cubic (fluorite) phase. Furthermore, the Raman spectrum of the as sprayed GZO/YbSZ (Fig. 3b, red curve) support the presence of a fluorite phase and demonstrate
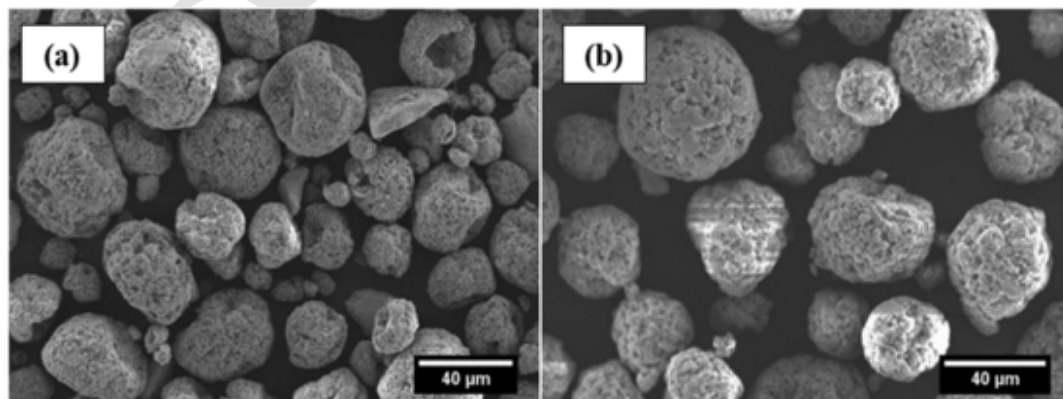
**Table 2**
Optimized parameters used for air plasma spraying (APS) of bondcoat and topcoat, respectively (*Standard liter per minute).

| Parameter | Bondcoat | Topcoat |
|---|---|---|
| Current (A) | 650 | 700 |
| Voltage (V) | 38 | 40 |
| Primary gas, Ar (SLPM*) | 28 | 24 |
| Secondary gas, $H_2$ (SLPM*) | 30 | 15 |
| Powder feed rate (g/min) | 35 | 30 |
| Spray distance (cm) | 10 | 8 |



**Fig. 1.** Morphology of spray dried powders (a) GZO, and (b) GZO/YbSZ.
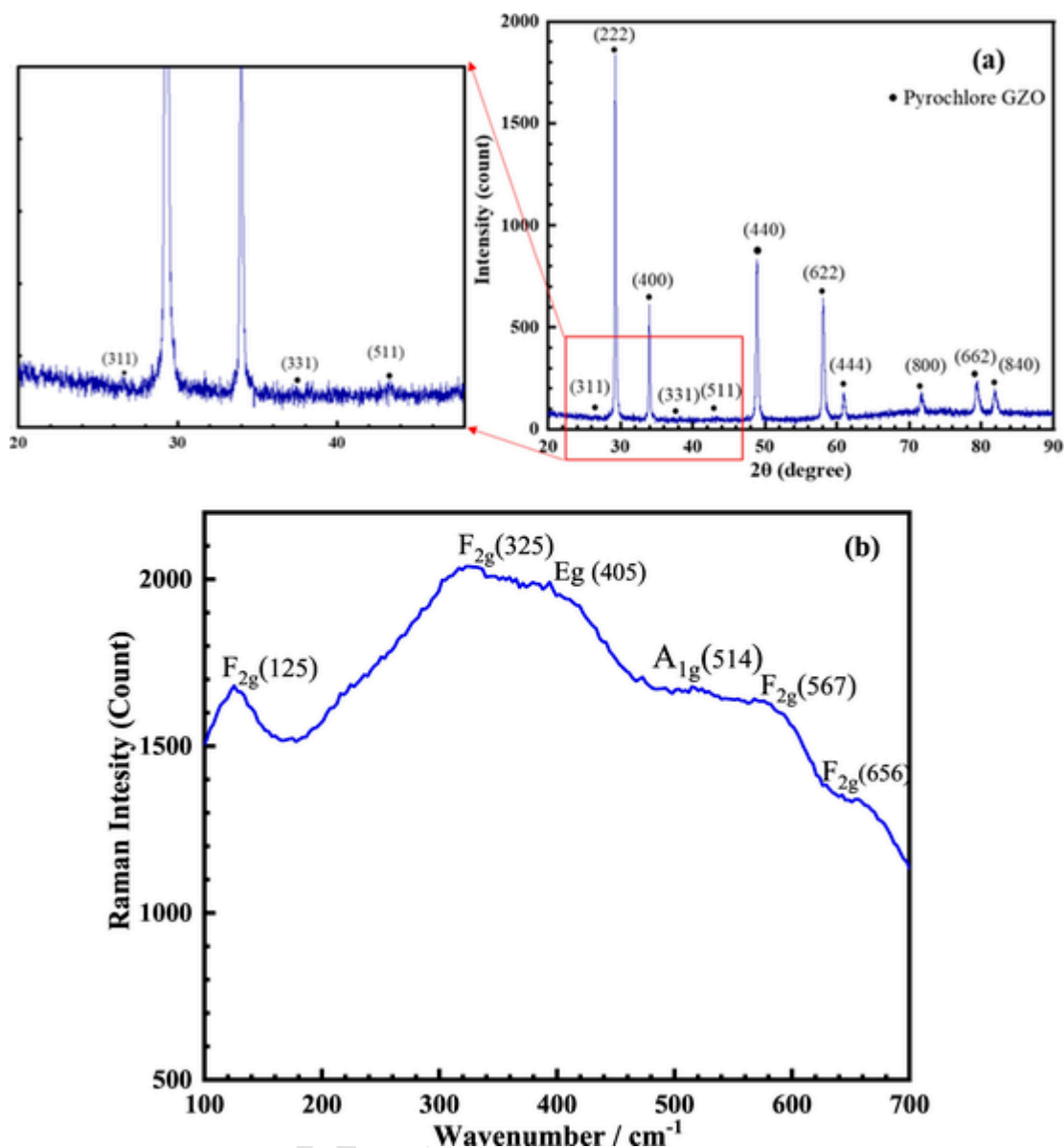
**Fig. 2.** (a) XRD pattern, and (b) Raman spectrum of the as-sprayed GZO coating. The Raman modes of the pyrochlore phase are included.

that a single phase is formed between GZO and YbSZ during plasma spraying.

The microstructure of the polished cross-sections and fracture surfaces of the different coatings are shown in Fig. 4. The plasma-sprayed coatings have a homogeneous thickness and microstructure and adhere well to the substrate. The different layers are clearly visible in Fig. 4a, c, e and g, including numbers for the thickness of the various coatings. The micrographs at higher magnification (Fig. 4b, d and f) show cracks, pores, splat boundaries and un-melted or semi-melted particles which are characteristic for plasma sprayed coatings. Cracks are usually due to thermal stresses and rapid solidification after plasma spraying [15].

The average fracture toughness of GZO, GZO/YbSZ and YSZ coatings were assessed to be $0.6 \pm 0.1$, $2.3 \pm 0.6$ and $1.2 \pm 0.3$ MPa·m$^{1/2}$, respectively. A representative SEM image of indented cross section of the GZO coating is shown in Fig. 4h. The individual results of each indentation are detailed in Table A1 in Appendix A.

### 3.3. Microstructure and characterization of the coatings after hot corrosion test

#### 3.3.1. GZO topcoat

The XRD patterns of the GZO coatings after hot corrosion tests for 3, 6, 12, 18 and 24 h are presented in Fig. 5, and GdVO$_4$ is the main hot corrosion product observed. The intensity of the GdVO$_4$ diffractions lines increases with time. Some monoclinic ZrO$_2$ is observed originating from GZO as it reacts with V, however the GZO is seen to mainly maintain its pyrochlore structure. Diffraction lines of Na$_2$SO$_4$ are observed from 6 h and correspond to insufficient reaction between Na$_2$SO$_4$ and V$_2$O$_5$ at 750 °C.

The SEM micrographs in Fig. 6 of the surface of the GZO coatings after the hot corrosion test for 3 and 24 h show that the size and quantity of the corrosion products were more pronounced with increasing hot corrosion time. From EDS analysis (Fig. A1), the rod-shaped crystals (point A in Fig. 6a) contain Gd and V (molar ratio 1:1) confirming the formation of GdVO$_4$. Point B in Fig. 6a mainly consists of Gd and
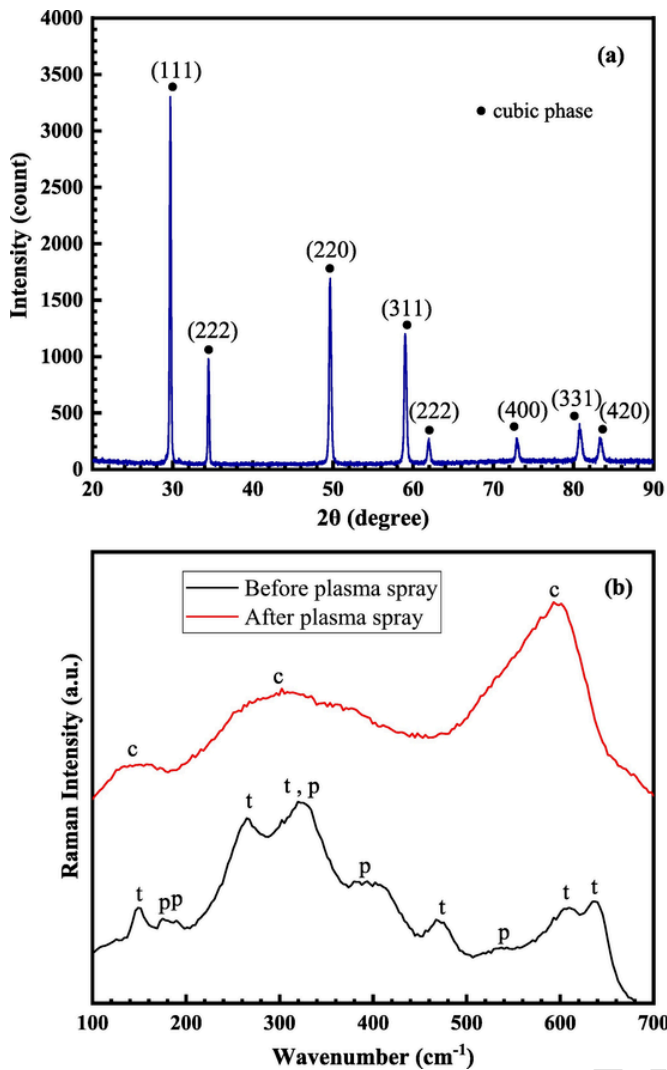
**Fig. 3.** (a) XRD pattern of as-sprayed GZO/YbSZ coating, (b) Black curve: Raman spectrum of GZO/YbSZ powder prior to plasma spraying (t: tetragonal and p: pyrochlore). Red curve: Raman spectrum of as-sprayed GZO/YbSZ coating (c: cubic). (For interpretation of the references to colour in this figure legend, the reader is referred to the web version of this article.)

Zr corresponding to GZO, however some Na and V is also detected due to the presence of the corrosive mixture.

It is anticipated that the thermally grown oxide layer (TGO) is formed early and that the thickness increases with time. The SEM micrographs of the polished cross-section of the GZO coating after the hot corrosion test for 24 h in Fig. 7a show the formation of a wide crack in the GZO close to the interface between the topcoat and the bondcoat and will be further explained in the discussion.

In the GZO coating, the TGO layer is formed continuously along the bondcoat/topcoat interface during the hot corrosion test (Fig. 8). The EDS analysis shows that the TGO layer mainly consists of Al and O confirming the formation of a thin ($\sim$2 μm) $Al_2O_3$ layer between topcoat and bondcoat after 12 h corrosion test.

### 3.3.2. GZO/YbSZ and YSZ + GZO/YbSZ topcoats

The XRD patterns of the GZO/YbSZ and YSZ + GZO/YbSZ coatings after hot corrosion test for 3, 6, 12, 18 and 24 h are given in Fig. 9. During the hot corrosion test, the molten salts penetrate through the coating via pores and cracks and monoclinic zirconia appears due to the depletion of $Gd_2O_3$ forming GdVO$_4$. Diffraction lines for $Na_2SO_4$ are present after 3 h due to incomplete reaction between $Na_2SO_4$ and $V_2O_5$.

Fig. 10 shows the rod-shaped GdVO$_4$ crystals on the GZO/YbSZ coating after hot corrosion tests for 3 and 24 h. By increasing the hot corrosion time, a larger amount of corrosion products was observed.

In contrast to the significant spallation and crack formation observed for the GZO topcoat after 24 h (Fig. 7a), the GZO/YbSZ topcoat (Fig. 11a) showed less severe crack formation after 24 h and spallation was not observed. The interface between the topcoat and bondcoat (Fig. 11b) also showed a coherent crack-free structure with the TGO formed in-between. The cross section of the double layer, YSZ + GZO/YbSZ, after 24 h hot corrosion test is shown in Fig. 11c. A coherent and crack-free interface is observed between GZO/YbSZ and YSZ, however a severe crack in the YSZ layer approx. 50 μm above the interface between the bondcoat and YSZ is evident. Nevertheless, the interface between YSZ and bondcoat seems to be coherent (Fig. 11c and d).

The main differences observed between the single-layer GZO/YbSZ and the double-layer YSZ + GZO/YbSZ coatings are the thickness and continuity of the TGO layer. In the GZO/YbSZ coating, the TGO layer is thin and partly discontinuous (Fig. 11b) while a thicker and continuous TGO is formed in combination with the YSZ + GZO/YbSZ coating (Fig. 11d). Hence, the GZO/YbSZ coating provides a better protection against oxidation of substrate.

### 3.3.3. YSZ topcoat

XRD patterns of the YSZ coating after hot corrosion test for 3, 6, 12, 18, and 24 h are presented in Fig. 12. YVO$_4$ is the dominant corrosion product observed and zirconia is partly transformed into the monoclinic phase already after 3 h. The intensity of the diffraction lines from YVO$_4$ and monoclinic zirconia is increasing with time.

Fig. 13 shows the SEM micrographs of the surface of the YSZ coating after 3 and 24 h, showing the increasing amount of rod-shaped YVO$_4$ crystals with time. Comparing corrosion behavior of GZO/YbSZ and YSZ after 24 h exposure (Fig. 10b and Fig. 13b) the corrosion is more severe in the case of a YSZ topcoat.

The interface cross-sectional images taken after 3 and 24 h hot corrosion tests of YSZ coating are given in Fig. 14 and shows that the TGO layer has been formed already after 3 h (dark gray areas in Fig. 14a). The formed TGO layer is dense, discontinuous and consists mainly of $Al_2O_3$ (Fig. A2). By increasing the hot corrosion time to 24 h (Fig. 14b) the TGO layer seems to be separated into a light gray- and a dark gray layer, corresponding to a Cr, Ni, Co enriched mixed oxide and an alumina rich TGO, respectively.

## 4. Discussion

### 4.1. Microstructure and fracture toughness of the as sprayed topcoats

SEM analysis of cross sections of the as-received plasma sprayed coatings given in Fig. 4, shows well defined interfaces and good adherence between the different phases, corresponding to samples well adapted for hot corrosion testing. The lowest porosity ($\sim$10–12%) was observed for the YSZ- and GZO/YbSZ coatings, whereas the highest porosity ($\sim$17%) was assessed for the GZO coating. Hence, the lowest sinterability is exhibited by GZO. It should be noted that during the plasma spraying the powders experience temperatures from 6000 to 15,000 °C, converting the powders to a liquid phase prior to deposition on the substrate [29]. Hence, the sintering mechanism is probably a combination of liquid- and solid-state sintering and inherently challenging to control.

The $K_{IC}$ for GZO/YbSZ reached 2.3 MPa·m$^{1/2}$, while $K_{IC}$ was reduced to 0.6 MPa·m$^{1/2}$ for GZO consistent with values reported elsewhere [30]. Hence adding 82 mol% YbSZ to GZO increase the fracture toughness by a factor of 3.8 compared with pure GZO. Zhang et al. [19] conducted a similar study and reported a fracture toughness of 1.9 MPa·m$^{1/2}$ for GZO doped with 40 mol% YbSZ (3.5 mol% Yb$_2$O$_3$ in ZrO$_2$). This clearly shows the beneficial effect of YbSZ with respect to
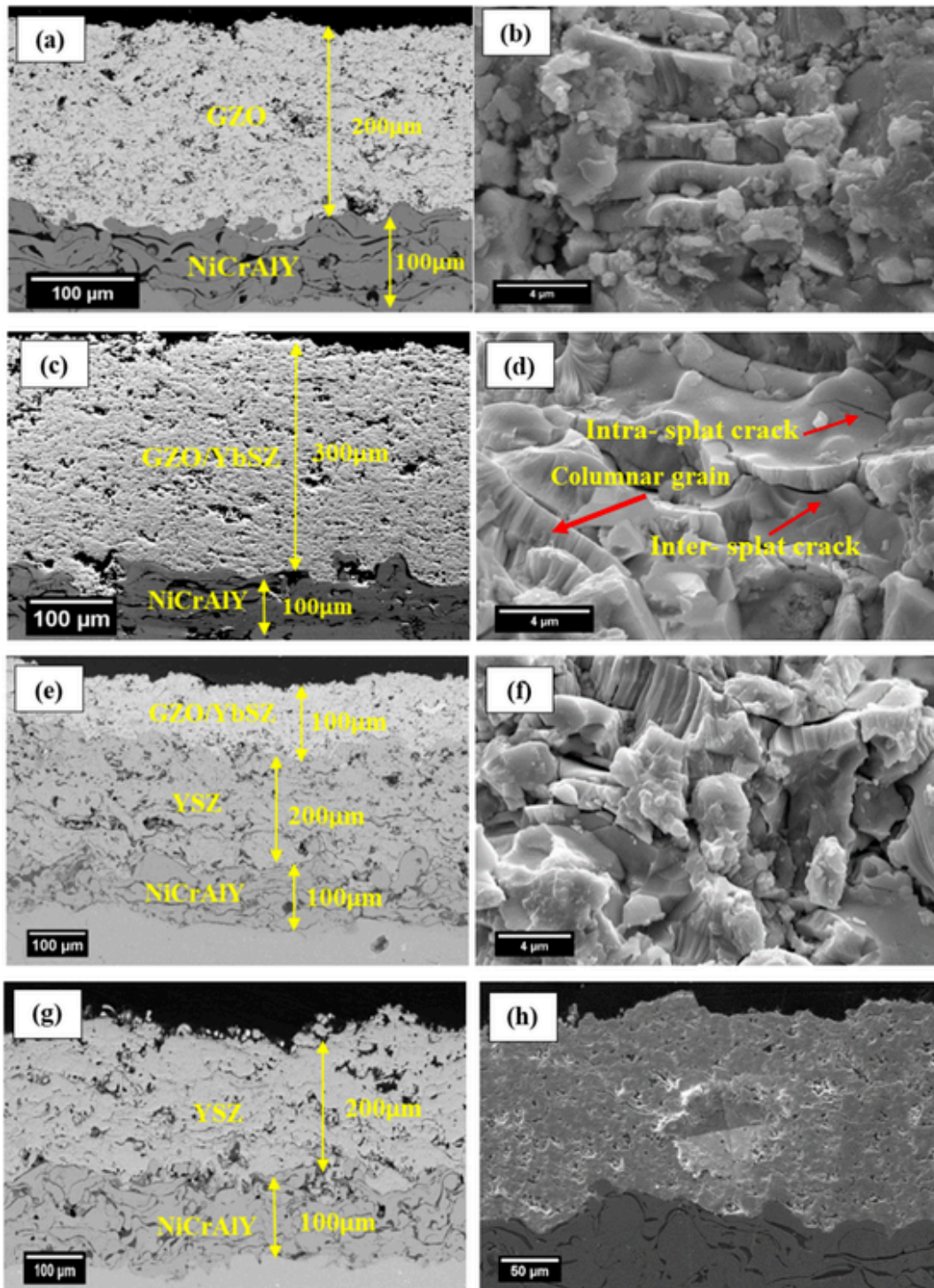
**Fig. 4.** SEM micrographs of polished cross sections and fracture surfaces of the different coatings (a and b) GZO, (c and d) GZO/YbSZ, (e and f) YSZ + GZO/YbSZ and (g) YSZ.(h) SEM image of Vickers indent of GZO coating.

the mechanical properties of GZO. The role of YbSZ, on enhancement of the fracture toughness, is not clear and somewhat unexpected considering the cubic structure of GZO/YbSZ. The reason might be a combination of a favorable microstructure (small grains) and increased bond strength as $Gd^{3+}$ is replaced by the smaller $Yb^{3+}$ in GZO/YbSZ [31]. A mechanism similar to transformation toughened zirconia may also be considered, however a confirmation needs a careful analysis of the phases present along the crack path and at the crack tip to detect whether formation of monoclinic $ZrO_2$ has taken place.

### 4.2. Plasma sprayed mixtures of GZO + YbSZ

Prior to plasma spraying, agglomerates of 1:1 (mass) mixtures of GZO and YbSZ was produced by spray drying (Fig. 1b). The YbSZ was converted to a tetragonal single phase by calcination at 800 °C (Fig. 3b, black curve) prior to mixing with GZO, which is in reasonable agreement with the phase diagram published by Fabrichnaya et al. [32]. According to Li et al. [26], GZO preserves its pyrochlore struc-
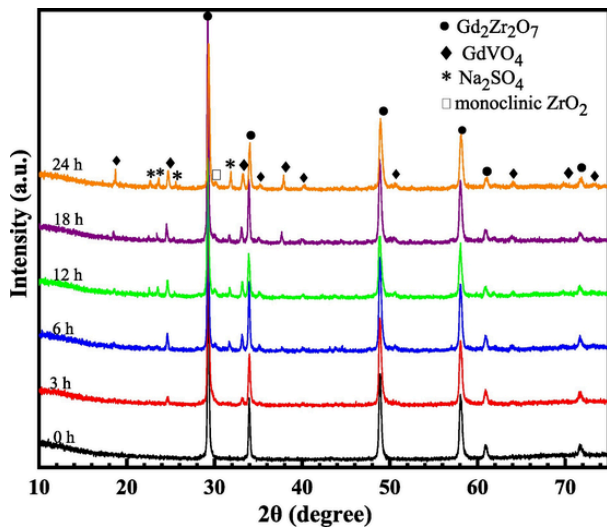
**Fig. 5.** XRD patterns of GZO coating after hot corrosion test at 750 °C for different times.

ture until approx. 1550 °C where a phase transition to a cubic phase (fluorite) takes place. However, there are no published phase diagrams for the entire $Gd_2O_3$-$ZrO_2$-$Yb_2O_3$ system. Nevertheless, our investigation shows that GZO/YbSZ forms a single-phase compound with fluorite structure, corresponding to a solid solution between $Gd_2O_3$, $ZrO_2$ and $Yb_2O_3$ at the prevailing temperature of plasma spraying and compositions with 82 mol% YbSZ. Zhang et al. [19] sintered samples with 40 mol% YbSZ in GZO at 1600 °C and based on Raman spectroscopy and XRD they reported a phase separation corresponding to a pyrochlore- and a tetragonal phase. According to our study compounds with 82 mol% YbSZ will stabilize the fluorite phase.
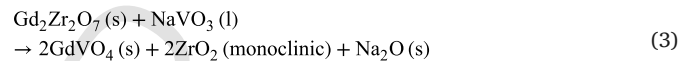
### 4.3. Hot corrosion testing

An equimolar mixture of $V_2O_5$ and $Na_2SO_4$ has been applied in the present investigation to test the corrosion properties of the topcoats. According to the phase diagram [15,27] $NaVO_3$ will form at elevated temperatures according to reaction (2).

$$Na_2SO_4 \text{ (s)} + V_2O_5 \text{ (l)} \rightarrow 2NaVO_3 \text{ (l)} + SO_3 \text{ (g)} \tag{2}$$
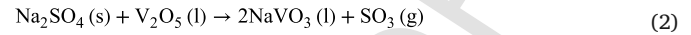
$NaVO_3$ melts congruently at $T > 610$ °C and given complete reaction between $Na_2SO_4$ and $V_2O_5$ the topcoats should in principle be exposed to liquid $NaVO_3$ at 750 °C. Post XRD analysis of the surfaces of all the topcoats shows however traces of $Na_2SO_4$ (Figs. 5, 9 and 12), due to insufficient reaction and/or inhomogeneous mixing of the reactants. The amount of $Na_2SO_4$ is nevertheless small, and the topcoat is assumed to be mainly exposed to liquid $NaVO_3$ during hot corrosion testing.

### 4.4. Formation of corrosion products during hot corrosion testing

From the XRD analysis of the topcoat surface after corrosion test, the formation of $GdVO_4$ and monoclinic $ZrO_2$ is observed for GZO (Fig. 5), GZO/YbSZ (Fig. 9a) and the double layered YSZ + GZO/YbSZ (Fig. 9b), due to reaction (3):

$$Gd_2Zr_2O_7 \text{ (s)} + NaVO_3 \text{ (l)}$$
$$\rightarrow 2GdVO_4 \text{ (s)} + 2ZrO_2 \text{ (monoclinic)} + Na_2O \text{ (s)} \tag{3}$$

Due to insufficient reaction between $Na_2SO_4$ and $V_2O_5$ (reaction (2)), the following reaction with $Gd_2Zr_2O_7$ forming $GdVO_4$ is also possible [6,17]:

$$Gd_2Zr_2O_7 \text{ (s)} + V_2O_5 \text{ (l)} \rightarrow 2GdVO_4 \text{ (s)}$$
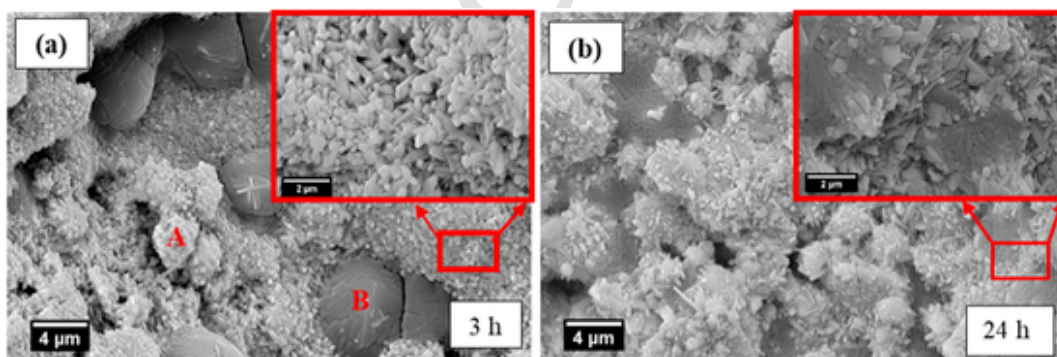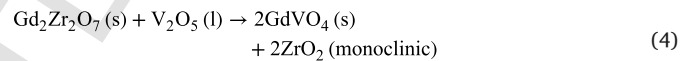$$+ 2ZrO_2 \text{ (monoclinic)} \tag{4}$$



**Fig. 6.** Surface morphologies of GZO coatings after hot corrosion test at 750 °C for 3 h (a) and 24 h (b). Images with different magnifications are given. EDS point analysis of A and B is given in Fig. A1.
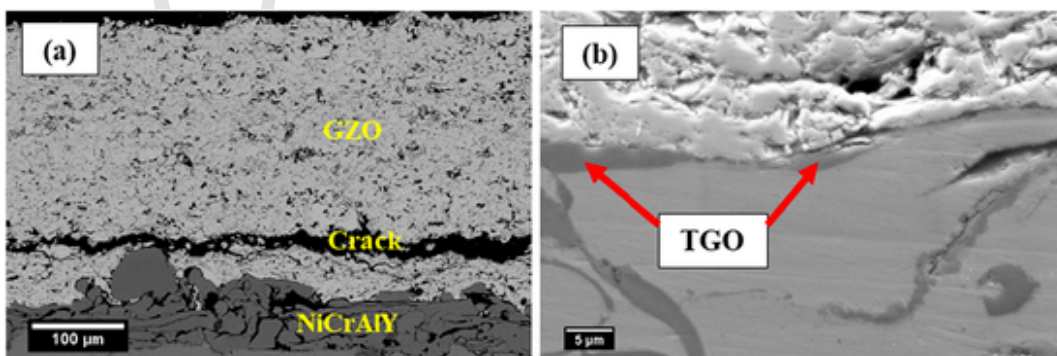


**Fig. 7.** (a and b) SEM micrographs of the cross-section of GZO coating after hot corrosion tests for 24 h (at two different magnifications).
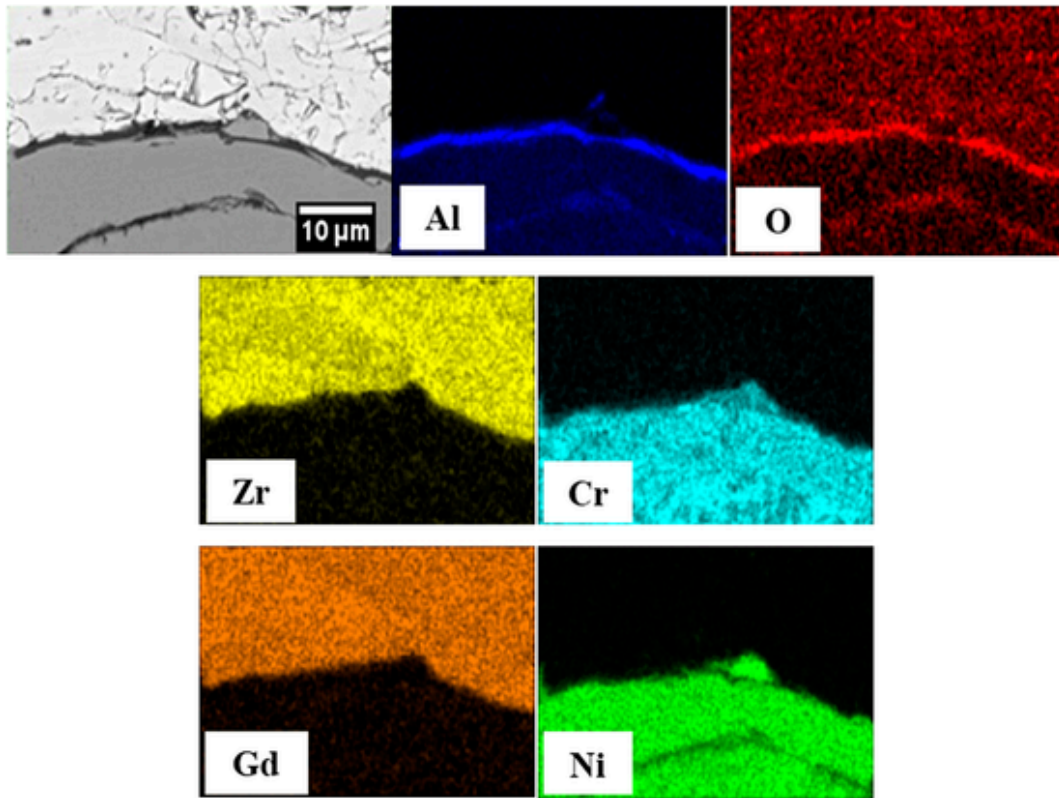
**Fig. 8.** Cross-sectional EDS elemental mapping analysis of the GZO coating after hot corrosion test for 12 h.

Habibi et al. indicated that reactions 3 and 4 are the main reactions taking place during hot corrosion of GZO and GZO + YSZ coatings [6].

Acidic vanadium oxide compounds will react with the more basic oxides. Moeller and Kremers [33] reported the basicity of $Gd_2O_3$ to be higher than $Yb_2O_3$, hence the molten $NaVO_3$ have a preference to react with $Gd_2O_3$ rather than $Yb_2O_3$. This is confirmed by the XRD patterns in Fig. 9 where the diffraction lines of $GdVO_4$ are observed. As Gd is leached out of either GZO or GZO/YbSZ, monoclinic zirconia is formed simultaneously. Due to high hygroscopicity $Na_2O$ was not detected by X-ray diffraction. However, whereas GZO seems to form increasing amounts of $GdVO_4$ with time (Fig. 5), significantly smaller amounts of $GdVO_4$ are formed at the surface of GZO/YbSZ (Fig. 9), and the amount is also seemingly independent of time. Based on these observations, GZO/YbSZ is less prone to corrosion compared with GZO and is possibly related to the reduced chemical potential of Gd in GZO/YbSZ due to the high amount of YbSZ (82 mol%).

The YSZ topcoat forms increasing amounts of $YVO_4$ and monoclinic $ZrO_2$ with time (Fig. 12) and the hot corrosion of YSZ can be described by reaction (5).

$$Zr_{1-x}Y_xO_{2-1.5x} + xNaVO_3\,(l)$$
$$\rightarrow xYVO_4\,(s) + (1-x)\,ZrO_2\,(monoclinic) \qquad (5)$$
$$+ 0.5xNa_2O\,(s)$$
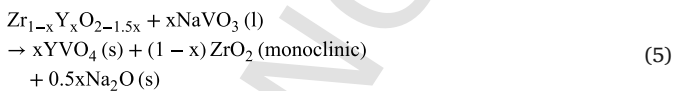
showing that yttria is the reactive component and forms the corrosion product. However, after 24 h corrosion a significant amount of m-$ZrO_2$ is formed in the YSZ coating (Fig. 12), whereas m-$ZrO_2$ is virtually absent in the GZO coating. The presence of m-$ZrO_2$ may add to the degradation of the coatings making zirconia more prone to failure as YSZ is destabilized when yttria is leached out. In this respect the GZO coating will exhibit a higher corrosion resistance than YSZ which is in accordance with the results reported by Habibi et al. [6].

### 4.5. Crack formation and spallation

The SEM analysis of the cross sections of the coatings given in Figs. 7, 11 and 14 shows a wide crack after 24 h in the GZO topcoat close to the interface between GZO and the bondcoat (Fig. 7). The adhesion between the topcoat and bondcoat is well established and it seems that the crack formation is due to thermal expansion mismatch between the topcoat and bondcoat. The values of the TEC of NiCrAlY is $\sim 15 \times 10^{-6}$ K$^{-1}$ and of GZO $\sim 8$–9 $\times 10^{-6}$ K$^{-1}$ at 1000 °C [4]. Hence, the differences in TECs lead to thermal stresses during heating and cooling and combined with the low fracture toughness of GZO ($\sim 0.6$ MPa·m$^{1/2}$, [4]) the topcoat is prone to crack formation and spallation. In addition, the GZO coating also exhibited the highest porosity among the topcoats which facilitates the penetration of the molten salts more easily and add to the degradation of the topcoat.

The cross section of the GZO/YbSZ coating shown in Fig. 11a also shows a crack in the topcoat close to the bondcoat, however in contrast to GZO the crack is less severe and even discontinuous. The highest fracture toughness among the topcoats was measured for GZO/YbSZ reaching $\sim 2.3$ MPa·m$^{1/2}$. Hence, the improved resistance against crack formation and spallation in GZO/YbSZ compared with pyrochlore structured GZO is assumed to be due to its enhanced fracture toughness combined with a higher corrosion resistance.

From the cross section of the double layered YSZ + GZO/YbSZ (Fig. 11c) a wide crack is observed in the YSZ phase close to the bondcoat. At higher magnification there is also an indication of less adherence between YSZ and the bondcoat (Fig. 11d). Although it is expected that the top layer of GZO/YbSZ will protect the YSZ against hot corrosion, the thermal expansion mismatch between the bondcoat and YSZ combined with the moderate fracture toughness of YSZ will form cracks.
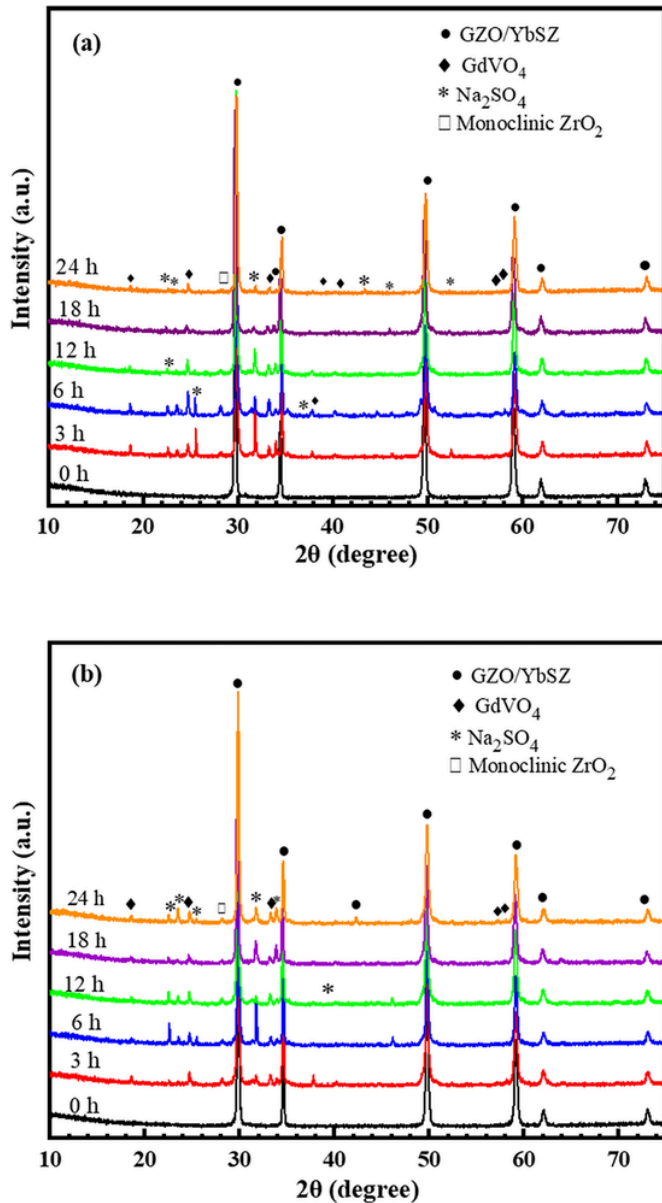
**Fig. 9.** XRD patterns of (a) GZO/YbSZ coating, and (b) YSZ + GZO/YbSZ coating after hot corrosion test for different times.

Further, for the YSZ coating (Fig. 14a) there is a good adherence between the topcoat and bondcoat after 3 h hot corrosion. However, after 24 h the TGO layer is separated in two layers (Fig. 14b), a dark gray (enriched with alumina) and a light gray (alumina mixed with Cr-, Co- and Ni-oxides). Lashmi et al. reported that spallation of YSZ was due to the formation of the TGO layer which involved the transformation of the high density metallic bondcoat to a low-density oxide and subsequent spallation [11]. It is also likely that the formation of $YVO_4$ and monoclinic $ZrO_2$ contributes to the deterioration of the YSZ topcoat.

### 4.6. Oxidation of the bond coat (TGO)

The formation of an oxide layer at the surface of the bondcoat is well documented in the results and according to Fig. 8 an alumina rich layer is formed. The TGO layer may be beneficial and protect the bondcoat against further oxidation as well as add to the bonding between topcoat and bondcoat [34,35]. For all the coatings investigated, the present study indicate that the molten salts cannot easily reach the bond coat and react with the TGO. It is reported that molten salts may react with alumina and finally lead to damage of the continuous alumina scale and degradation of the TBC [25]. In the present investigation there was no clear evidence of penetration of the molten salt to the TGO layer and it is concluded that the plasma sprayed coatings gave a good protection with respect to avoiding interaction between the molten salts and the TGO layers.

Based on our investigation, GZO/YbSZ is a promising candidate for topcoat applications, due to its reduced reactivity at hot corrosion conditions combined with an enhanced fracture toughness. A fruitful follow up of the present study would be a further investigation into the system $Gd_2Zr_2O_7$-YbSZ aiming at improving the mechanical properties even more at high temperatures.

### 5. Conclusion

In this study, a new composition with 50 wt% (82 mol%) YbSZ in GZO has been investigated as an alternative ceramic topcoat. The hot corrosion properties of GZO/YbSZ were compared with commercial and traditional YSZ coatings as well as GZO and double-layer YSZ + GZO/YbSZ coatings. Prior to hot corrosion the fracture toughness of the coatings was assessed by Vickers indentation showing $0.6 \pm 0.1$, $1.2 \pm 0.3$ and $2.3 \pm 0.6$ MPa·m$^{1/2}$ for GZO, YSZ and GZO/YbSZ respectively.

The coatings were exposed to hot corrosion by an equimolar mixture of $Na_2SO_4$ and $V_2O_5$ at 750 °C. Single layer GZO/YbSZ showed the best resistance against corrosion followed by YSZ + GZO/YbSZ coatings. After hot corrosion tests, rod-shaped $GdVO_4$ crystals along with monoclinic $ZrO_2$ were formed on the surface of the GZO, GZO/YbSZ
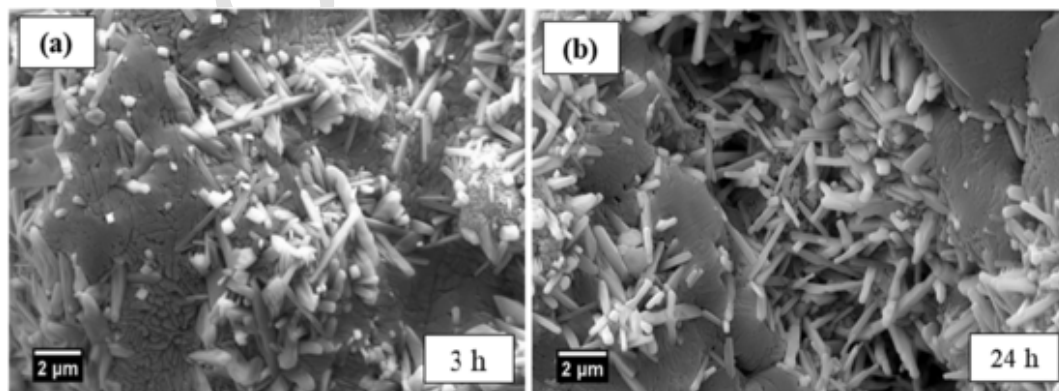


**Fig. 10.** Surface morphologies of GZO/YbSZ after hot corrosion test for 3 h (a) and 24 h (b) at 750 °C.
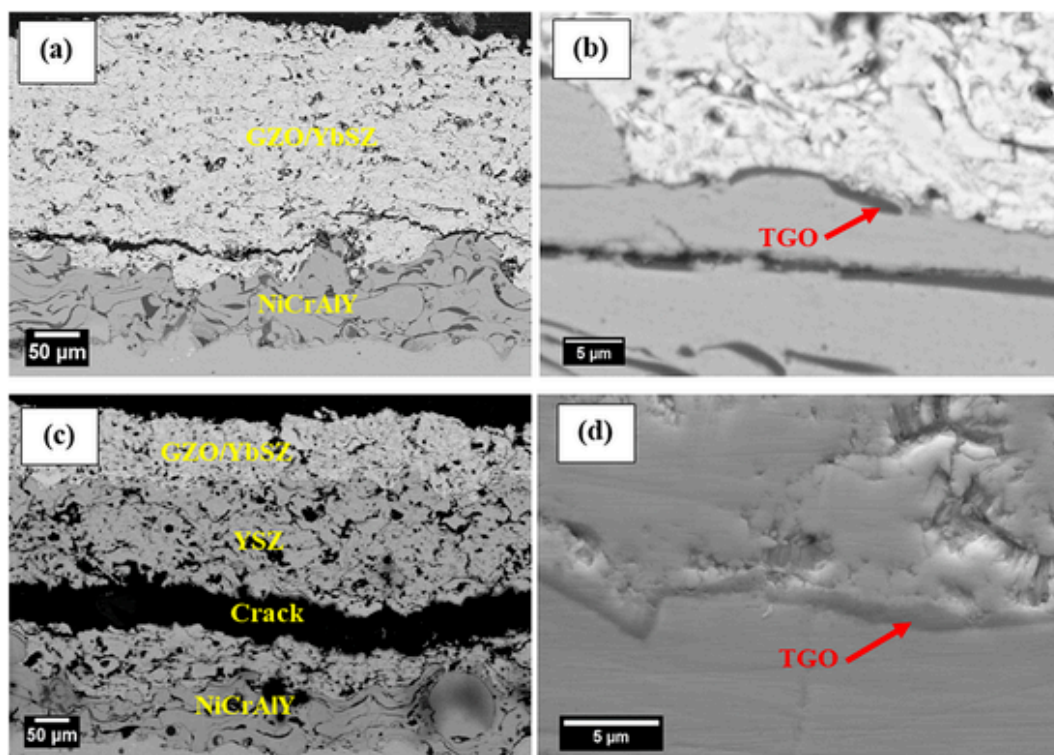
**Fig. 11.** SEM micrographs of the cross-section of (a and b) GZO/YbSZ coating and (c and d) YSZ + GZO/YbSZ coating, respectively after 24 h hot corrosion test. Images with different magnifications are given.
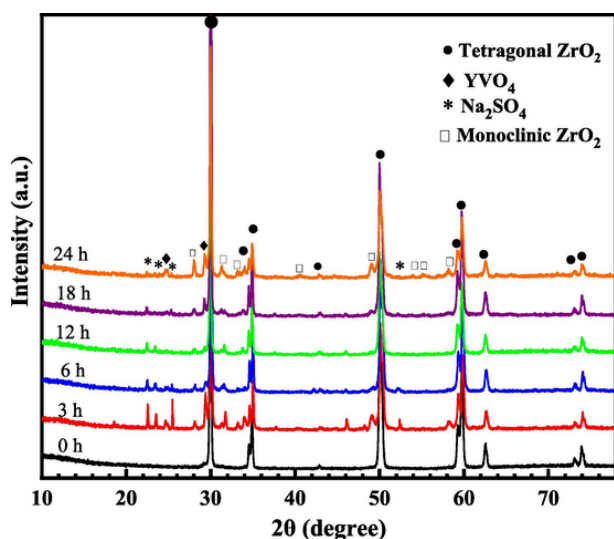


**Fig. 12.** XRD patterns of YSZ coating after hot corrosion test for different times.

and YSZ + GZO/YbSZ coatings, while monoclinic zirconia and $YVO_4$ were the main corrosion products of the YSZ coating. Highest amount of corrosion products was observed for YSZ. The formation and growth of the TGO layer occurred in all coatings, but with different thicknesses. However, wide cracks were observed in all coatings except for GZO/YbSZ where only a narrow and discontinuous crack was observed. Based on the observations the best coating for TBC applications is GZO/YbSZ due to its reduced reactivity at hot corrosion conditions combined with an enhanced fracture toughness.

## Uncited references

[36–40]

## CRediT authorship contribution statement

**Mohadese Tabeshfar:** Investigation, Writing - original draft. **Mehdi Salehi:** Conceptualization, Methodology, Project administration, Supervision, Funding acquisition, Validation. **Ghasem Dini:** Supervision. **Paul Inge Dahl:** Resources. **Mari-Ann Einarsrud:** Supervision, Writing - review & editing. **Kjell Wiik:** Resources, Funding acquisition, Project administration, Supervision, Methodology, Writing - review & editing.

## Declaration of competing interest

The authors declare that they have no known competing financial interests or personal relationships that could have appeared to influence the work reported in this paper.

## Acknowledgements

## Appendix A.

**Table A1**
Detailed results from 5 independent indents on each topcoat. The symbols are defined in Section 2.5.

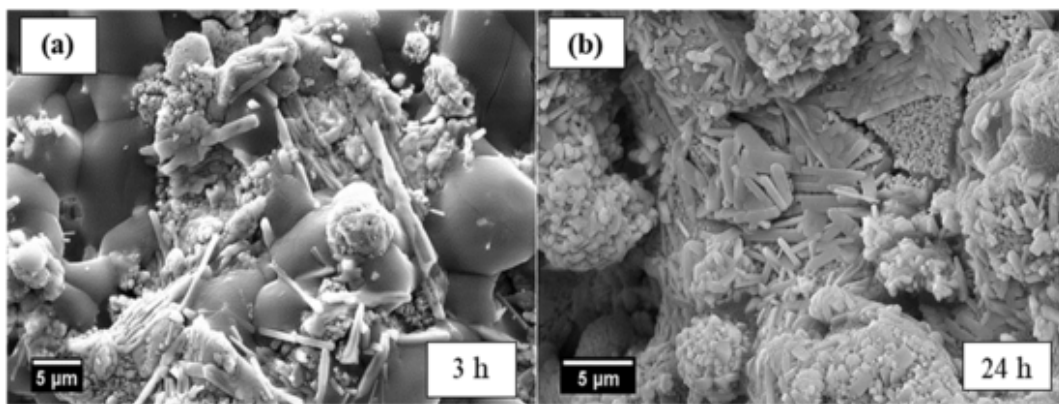| Compound | a(μm) | c(μm) | Hv(MPa) | $K_{IC}$(MPa$\sqrt{m}$) | $K_{IC, average}$ (MPa$\sqrt{m}$) |
|---|---|---|---|---|---|
| GZO | 84 | 176 | 1402 | 0.68 | 0.6 ± 0. |
|  | 73 | 169.5 | 1584 | 0.61 |  |
|  | 44 | 128 | 2216 | 0.47 |  |
|  | 30.5 | 96 | 4237 | 0.67 |  |

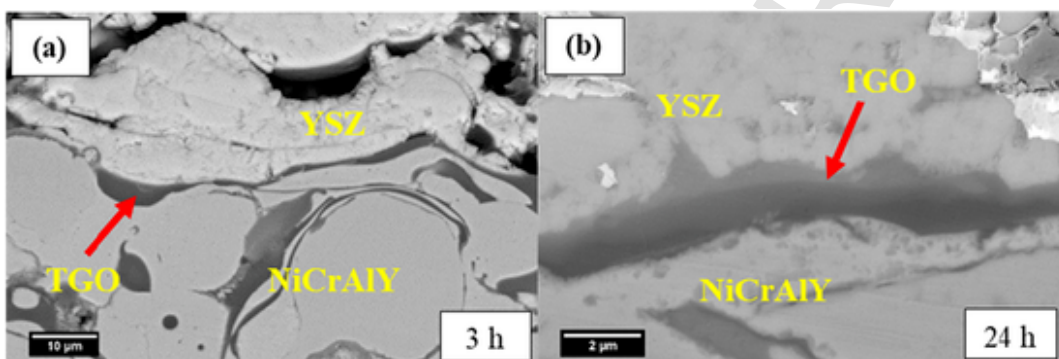**Fig. 13.** Surface morphologies of YSZ coating after 3 h (a) and 24 h (b) hot corrosion tests at 750 ˚C.



**Fig. 14.** SEM micrographs of the TGO layer of YSZ coating after hot corrosion test for 3 h (a) and 24 h (b).

| | | | | | | | | | | |
|---|---|---|---|---|---|---|---|---|---|---|
| | 33.2 | 99.1 | 4292 | 0.85 | | YSZ | 35 | 71 | 5217 | 1.7 | 1. |
| GZO/YbSZ | 30 | 56 | 5688 | 1.9 | 2. | | 38 | 101.5 | 3452 | 0.78 |
| | 32 | 44.5 | 5894 | 3.2 | | | 41 | 90 | 4237 | 1.3 |
| | 28 | 52.2 | 5129 | 1.7 | | | 39 | 86 | 3707 | 1.1 |
| | 31 | 58 | 5772 | 2 | | | 35 | 80 | 4649 | 1.3 |
| | 33 | 55.3 | 5698 | 2.4 | | | | | | |

| Element | Atomic% |
|---|---|
| Vanadium | 8 |
| Oxygen | 33.9 |
| Gadolinium | 9 |
| Total | 100 |

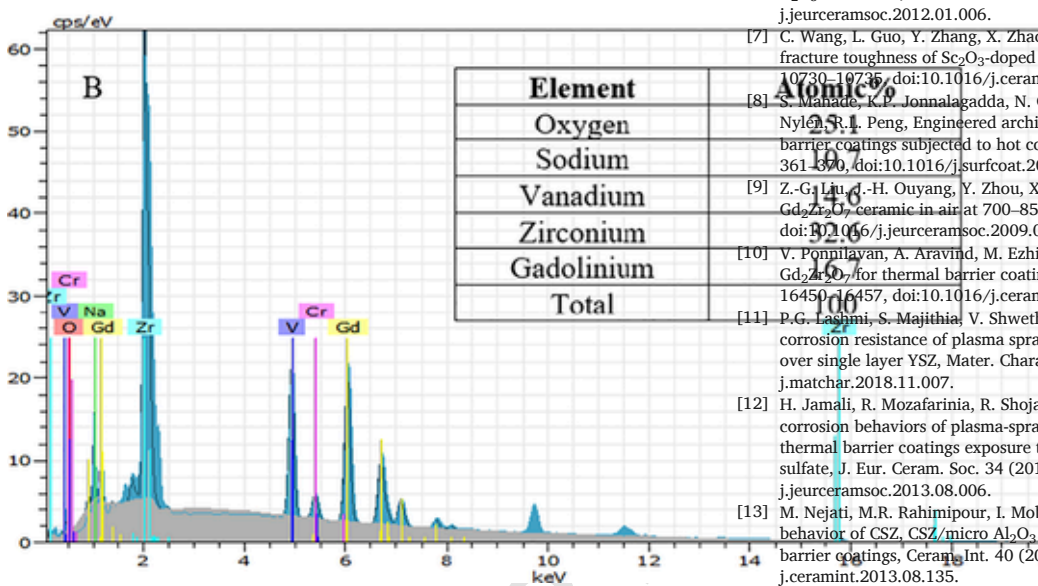| Element | Atomic% |
|---|---|
| Oxygen | 1 |
| Sodium | |
| Vanadium | 6 |
| Zirconium | |
| Gadolinium | |
| Total | 100 |

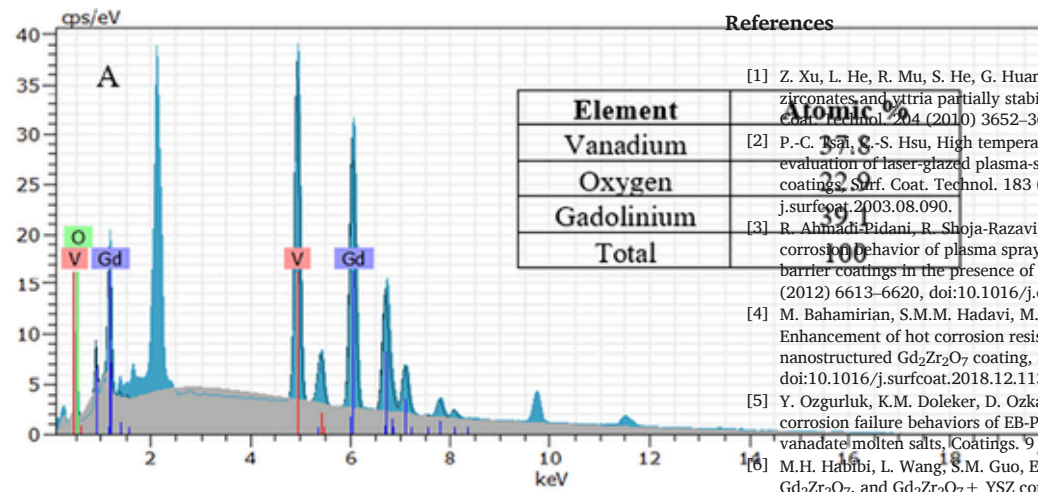**Fig. A1.** EDS analysis of point A and B as shown in Fig. 6a. Emphasis on some elements summed up to 100% to clarify the ratio between them.

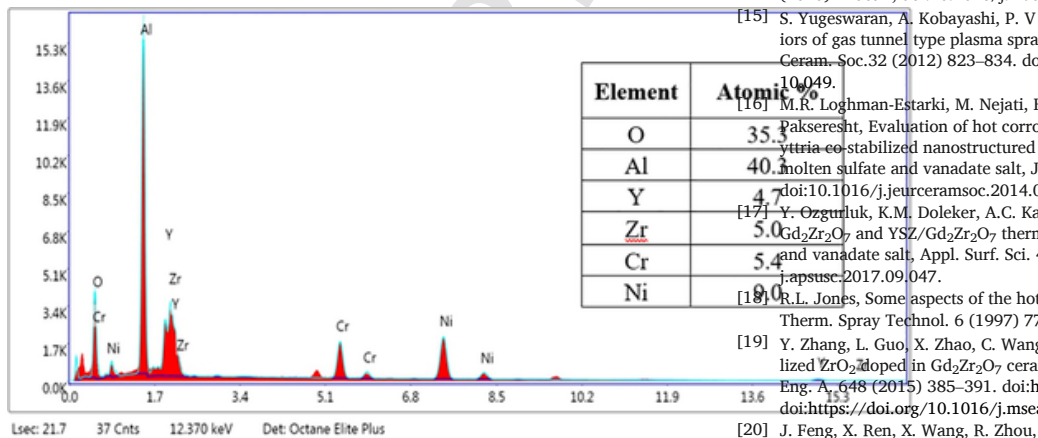| Element | Atomic% |
|---|---|
| O | 35.3 |
| Al | 40.3 |
| Y | 4.7 |
| Zr | 5.0 |
| Cr | 5.4 |
| Ni | |

**Fig. A2.** EDS analysis of TGO layer marked in Fig. 14a.

## References

[1] Z. Xu, L. He, R. Mu, S. He, G. Huang, X. Cao, Hot corrosion behavior of rare earth zirconates and yttria partially stabilized zirconia thermal barrier coatings, Surf. Coat. Technol. 204 (2010) 3652–3661, doi:10.1016/j.surfcoat.2010.04.044.

[2] P.-C. Tsai, J.-S. Hsu, High temperature corrosion resistance and microstructural evaluation of laser-glazed plasma-sprayed zirconia/MCrAlY thermal barrier coatings, Surf. Coat. Technol. 183 (2004) 29–34, doi:10.1016/j.surfcoat.2003.08.090.

[3] R. Ahmadi-Pidani, R. Shoja-Razavi, R. Mozafarinia, H. Jamali, Evaluation of hot corrosion behavior of plasma sprayed ceria and yttria stabilized zirconia thermal barrier coatings in the presence of $Na_2SO_4 + V_2O_5$ molten salt, Ceram. Int. 38 (2012) 6613–6620, doi:10.1016/j.ceramint.2012.05.047.

[4] M. Bahamirian, S.M.M. Hadavi, M. Farvizi, M.R. Rahimipour, A. Keyvani, Enhancement of hot corrosion resistance of thermal barrier coatings by using nanostructured $Gd_2Zr_2O_7$ coating, Surf. Coat. Technol. 360 (2019) 1–12, doi:10.1016/j.surfcoat.2018.12.113.

[5] Y. Ozgurluk, K.M. Doleker, D. Ozkan, H. Ahlatci, A.C. Karaoglanli, Cyclic hot corrosion failure behaviors of EB-PVD TBC systems in the presence of sulfate and vanadate molten salts, Coatings. 9 (2019) 166, doi:10.3390/coatings9030166.

[6] M.H. Habibi, L. Wang, S.M. Guo, Evolution of hot corrosion resistance of YSZ, $Gd_2Zr_2O_7$, and $Gd_2Zr_2O_7 + $ YSZ composite thermal barrier coatings in $Na_2SO_4 + V_2O_5$ at 1050° C, J. Eur. Ceram. Soc. 32 (2012) 1635–1642, doi:10.1016/j.jeurceramsoc.2012.01.006.

[7] C. Wang, L. Guo, Y. Zhang, X. Zhao, F. Ye, Enhanced thermal expansion and fracture toughness of $Sc_2O_3$-doped $Gd_2Zr_2O_7$ ceramics, Ceram. Int. 41 (2015) 10730–10735, doi:10.1016/j.ceramint.2015.05.008.

[8] S. Mahade, K.P. Jonnalagadda, N. Curry, X.-H. Li, S. Björklund, N. Markocsan, P. Nylén, R.L. Peng, Engineered architectures of gadolinium zirconate based thermal barrier coatings subjected to hot corrosion test, Surf. Coat. Technol. 328 (2017) 361–370, doi:10.1016/j.surfcoat.2017.09.005.

[9] Z.-G. Liu, J.-H. Ouyang, Y. Zhou, X.-L. Xia, Hot corrosion behavior of $V_2O_5$-coated $Gd_2Zr_2O_7$ ceramic in air at 700–850° C, J. Eur. Ceram. Soc. 29 (2009) 2423–2427, doi:10.1016/j.jeurceramsoc.2009.01.001.

[10] V. Ponnilavan, A. Aravind, M. Ezhilan, S. Kannan, Titanium substitution in $Gd_2Zr_2O_7$ for thermal barrier coating applications, Ceram. Int. 45 (2019) 16450–16457, doi:10.1016/j.ceramint.2019.05.176.

[11] P.G. Lashmi, S. Majithia, V. Shwetha, N. Balaji, S.T. Aruna, Improved hot corrosion resistance of plasma sprayed YSZ/$Gd_2Zr_2O_7$ thermal barrier coating over single layer YSZ, Mater. Charact. 147 (2019) 199–206, doi:10.1016/j.matchar.2018.11.007.

[12] H. Jamali, R. Mozafarinia, R. Shoja-Razavi, R. Ahmadi-Pidani, Comparison of hot corrosion behaviors of plasma-sprayed nanostructured and conventional YSZ thermal barrier coatings exposure to molten vanadium pentoxide and sodium sulfate, J. Eur. Ceram. Soc. 34 (2014) 485–492, doi:10.1016/j.jeurceramsoc.2013.08.006.

[13] M. Nejati, M.R. Rahimipour, I. Mobasherpour, Evaluation of hot corrosion behavior of CSZ, CSZ/micro $Al_2O_3$ and CSZ/nano $Al_2O_3$ plasma sprayed thermal barrier coatings, Ceram. Int. 40 (2014) 4579–4590, doi:10.1016/j.ceramint.2013.08.135.

[14] A.C. Karaoglanli, K.M. Doleker, Y. Ozgurluk, Interface failure behavior of yttria stabilized zirconia (YSZ), $La_2Zr_2O_7$, $Gd_2Zr_2O_7$, YSZ/$La_2Zr_2O_7$ and YSZ/$Gd_2Zr_2O_7$ thermal barrier coatings (TBCs) in thermal cyclic exposure, Mater. Charact. 159 (2020) 110072, doi:10.1016/j.matchar.2019.110072.

[15] S. Yugeswaran, A. Kobayashi, P. V Ananthapadmanabhan, Hot corrosion behaviors of gas tunnel type plasma sprayed $La_2Zr_2O_7$ thermal barrier coatings, J. Eur. Ceram. Soc.32 (2012) 823–834. doi:https://doi.org/10.1016/j.jeurceramsoc.2011.10.049.

[16] M.R. Loghman-Estarki, M. Nejati, H. Edris, R.S. Razavi, H. Jamali, A.H. Pakseresht, Evaluation of hot corrosion behavior of plasma sprayed scandia and yttria co-stabilized nanostructured thermal barrier coatings in the presence of molten sulfate and vanadate salt, J. Eur. Ceram. Soc. 35 (2015) 693–702, doi:10.1016/j.jeurceramsoc.2014.08.029.

[17] Y. Ozgurluk, K.M. Doleker, A.C. Karaoglanli, Hot corrosion behavior of YSZ, $Gd_2Zr_2O_7$ and YSZ/$Gd_2Zr_2O_7$ thermal barrier coatings exposed to molten sulfate and vanadate salt, Appl. Surf. Sci. 438 (2018) 96–113, doi:10.1016/j.apsusc.2017.09.047.

[18] R.L. Jones, Some aspects of the hot corrosion of thermal barrier coatings, J. Therm. Spray Technol. 6 (1997) 77–84, doi:10.1007/BF02646315.

[19] Y. Zhang, L. Guo, X. Zhao, C. Wang, F. Ye, Toughening effect of $Yb_2O_3$ stabilized $ZrO_2$ doped in $Gd_2Zr_2O_7$ ceramic for thermal barrier coatings, Mater. Sci. Eng. A. 648 (2015) 385–391. doi:https://doi.org/10.1016/j.msea.2015.09.081. doi:https://doi.org/10.1016/j.msea.2015.09.081.

[20] J. Feng, X. Ren, X. Wang, R. Zhou, W. Pan, Thermal conductivity of ytterbia-stabilized zirconia, Scr. Mater. 66 (2012) 41–44, doi:10.1016/j.scriptamat.2011.09.038.

[21] K. Jiang, S. Liu, Thermophysical Properties and Sintering of Ytterbia-Stabilized Tetragonal Zirconia Ceramic, Adv. Eng. Mater. 17 (2015) 21–27, doi:10.1002/adem.201400065.

[22] L. Guo, C. Zhang, L. Xu, M. Li, Q. Wang, F. Ye, C. Dan, V. Ji, Effects of $TiO_2$ doping on the defect chemistry and thermo-physical properties of $Yb_2O_3$ stabilized $ZrO_2$, J. Eur. Ceram. Soc. 37 (2017) 4163–4169, doi:10.1016/j.jeurceramsoc.2017.04.065.

[23] J. Yu, C. Wang, Y. Yu, Q. Yuan, Y. Tan, Z. Feng, Hot corrosion behavior of $Y_4Al_2O_9$ ceramics for thermal barrier coatings exposed to calcium-magnesium-alumina-silicate at 1250° C, J. Eur. Ceram. Soc. 39 (2019) 1487–1495, doi:10.1016/j.jeurceramsoc.2018.10.034.

[24] B.R. Marple, J. Voyer, M. Thibodeau, D.R. Nagy, R. Vassen, Hot corrosion of lanthanum zirconate and partially stabilized zirconia thermal barrier coatings, J. Eng. Gas Turbines Power. Jan 2006, 128(1)(2006)144–152. doi:https://doi.org/10.1115/1.1924534.

[25] K.P. Jonnalagadda, S. Mahade, S. Kramer, P. Zhang, N. Curry, X.-H. Li, R.L. Peng, Failure of Multilayer Suspension Plasma Sprayed Thermal Barrier Coatings in the Presence of $Na_2SO_4$ and NaCl at 900° C, J. Therm. Spray Technol. 28 (2019) 212–222, doi:10.1007/s11666-018-0780-5.

[26] M. Li, L. Guo, F. Ye, Phase structure and thermal conductivities of $Er_2O_3$ stabilized $ZrO2$ toughened $Gd_2Zr_2O_7$ ceramics for thermal barrier coatings, Ceram. Int. 42 (2016) 16584–16588, doi:10.1016/j.ceramint.2016.07.079.

[27] P. Mohan, B. Yuan, T. Patterson, V.H. Desai, Y.H. Sohn, Degradation of yttria-stabilized zirconia thermal barrier coatings by vanadium pentoxide, phosphorous pentoxide, and sodium sulfate, J. Am. Ceram. Soc. 90 (2007) 3601–3607, doi:10.1111/j.1551-2916.2007.01941.x.

[28] B.P. Mandal, N. Garg, S.M. Sharma, A.K. Tyagi, Solubility of $ThO_2$ in $Gd_2Zr_2O_7$ pyrochlore: XRD, SEM and Raman spectroscopic studies, J. Nucl. Mater. 392 (2009) 95–99, doi:10.1016/j.jnucmat.2009.03.050.

[29] J.R. Davis, Handbook of thermal spray technology ASM international 2004.

[30] M. Bahamirian, S.M.M. Hadavi, M. Farvizi, M.R. Rahimipour, A. Keyvani, Enhancement of hot corrosion resistance of thermal barrier coatings by using nanostructured $Gd_2 Zr_2O_7$ coating, Surf. Coat. Technol. 360 (2019) 1–12, doi:10.1016/j.surfcoat.2018.12.113.

[31] L. Ma, W. Ma, X. Sun, L. Ji, J. Liu, K. Hang, Microstructures and mechanical properties of $Gd_2Zr_2O_7/ZrO_2$ (3Y) ceramics, J. Alloys Compd. 644 (2015) 416–422, doi:10.1016/j.jallcom.2015.05.054.

[32] O. Fabrichnaya, S.M. Lakiza, M.J. Kriegel, J. Seidel, G. Savinykh, G. Schreiber, New experimental investigations of phase relations in the $Yb_2O_3$–$Al_2O_3$ and $ZrO_2$ –$Yb_2O_3$–$Al_2O_3$ systems and assessment of thermodynamic parameters, J. Eur. Ceram. Soc. 35 (2015) 2855–2871, doi:10.1016/j.jeurceramsoc.2015.03.037.

[33] T. Moeller, H.E. Kremers, Observations on the Rare Earths. LI. An Electrometric Study of the Precipitation of Trivalent Hydrous Rare Earth Oxides or Hydroxides., The . Phys. Chem. 48 (1944) 395–406. doi:https://doi.org/10.1021/j150438a004.

[34] A.C. Karaoglanli, E. Altuncu, I. Ozdemir, A. Turk, F. Ustel, Structure and durability evaluation of YSZ+ $Al_2O_3$ composite TBCs with APS and HVOF bond coats under thermal cycling conditions, Surf. Coat. Technol. 205 (2011) S369–S373, doi:10.1016/j.surfcoat.2011.04.081.

[35] K.M. Doleker, Y. Ozgurluk, H. Ahlatci, A.C. Karaoglanli, Evaluation of oxidation and thermal cyclic behavior of YSZ, $Gd_2Zr_2O_7$ and YSZ/$Gd_2Zr_2O_7$ TBCs, Surf. Coat. Technol. 371 (2019) 262–275, doi:10.1016/j.surfcoat.2018.11.055.

[36] E. Bakan, D.E. Mack, G. Mauer, R. Mücke, R. Vaßen, Porosity–property relationships of plasma-sprayed $Gd_2Zr_2O_7/$YSZ thermal barrier coatings, J. Am. Ceram. Soc. 98 (2015) 2647–2654, doi:10.1111/jace.13611.

[37] E. Bakan, R. Vaßen, Ceramic top coats of plasma-sprayed thermal barrier coatings: materials, processes, and properties, J. Therm. Spray Technol. 26 (2017) 992–1010, doi:10.1007/s11666-017-0597-7.

[38] N. Curry N. Markocsan L. Östergren X.-H. Li M. Dorfman Evaluation of the lifetime and thermal conductivity of dysprosia-stabilized thermal barrier coating systems J. Therm. Spray Technol. 22 2013 864 872 https://doi https://doi.org/10.1007/s11666-013-9932-9

[39] K.S. Lee, K.I. Jung, Y.S. Heo, T.W. Kim, Y.G. Jung, U. Paik, Thermal and mechanical properties of sintered bodies and EB-PVD layers of $Y_2O_3$ added $Gd_2Zr_2O_7$ ceramics for thermal barrier coatings, J. Alloys Compd. 507 (2010) 448–455, doi:10.1016/j.jallcom.2010.07.196.

[40] D. Lee, T.W. Kim, K.S. Lee, Design of thermal barrier coatings using gadolinium zirconate ceramics: A study on gadolinium zirconate/YSZ bilayers, J. Ceram. Soc. Japan. 117 (2009) 550–554, doi:10.2109/jcersj2.117.550.